Hindawi Publishing Corporation
Advances in Materials Science and Engineering
Volume 2015, Article ID 353140, 6 pages
http://dx.doi.org/10.1155/2015/353140

Research Article

The Microstructures and Electrical Resistivity of (Al, Cr, Ti)FeCoNiO_x High-Entropy Alloy Oxide Thin Films

Chun-Huei Tsau,[1] Zhang-Yan Hwang,[1] and Swe-Kai Chen[2]

[1]*Graduate School of Nanomaterials, Chinese Culture University, Taipei 111, Taiwan*
[2]*Materials Science Center, National Tsing Hua University, Hsinchu 300, Taiwan*

Correspondence should be addressed to Chun-Huei Tsau; chtsau@staff.pccu.edu.tw

Received 6 November 2014; Revised 9 December 2014; Accepted 9 December 2014

Academic Editor: Yong Zhang

The (Al, Cr, Ti)FeCoNi alloy thin films were deposited by PVD and using the equimolar targets with same compositions from the concept of high-entropy alloys. The thin films became metal oxide films after annealing at vacuum furnace for a period; and the resistivity of these thin films decreased sharply. After optimum annealing treatment, the lowest resistivity of the FeCoNiO_x, CrFeCoNiO_x, AlFeCoNiO_x, and TiFeCoNiO_x films was 22, 42, 18, and 35 $\mu\Omega$-cm, respectively. This value is close to that of most of the metallic alloys. This phenomenon was caused by delaminating of the alloy oxide thin films because the oxidation was from the surfaces of the thin films. The low resistivity of these oxide films was contributed to the nonfully oxidized elements in the bottom layers and also vanishing of the defects during annealing.

1. Introduction

This study deals with the room-temperature resistivity of alloy oxide thin films. In our previous study on the high-entropy alloy, TiFeCoNiO_x film had an extremely low resistivity (~35 $\mu\Omega$-cm) at room temperature [1, 2]. The value is almost close to that of metallic alloy, and it broke our concept that the alloy oxides had higher resistivity. Because the conductivity of semiconductors is much less than that of most metals, their resistivity was in the range between 10^5 and 10^{14} $\mu\Omega$-cm [3–5]. The design of the alloy targets of this study exploits Professor Yeh's equimolar alloy concept. Professor Yeh introduced the new concept of high-entropy alloys as basis for alloys whose properties are not dominated by their major element [6–12]. We used this concept to cast the TiFeCoNi alloy and studied its characteristics [13]; also we used this alloy as the target to measure the resistivity of the TiFeCoNiO_x thin film. In this study, we investigated the FeCoNiO_x, AlFeCoNiO_x, and CrFeCoNiO_x alloy oxide films, and the results were compared with TiFeCoNiO_x films. The FeCoNiO_x film was studied for estimating the effect of absence of titanium content. Additionally, we used aluminum to substitute titanium and studied AlFeCoNiO_x film, because the elements of aluminum and titanium had similar activity [14]. We also added chromium to substitute titanium because of its excellent oxidation resistance.

2. Experimental Procedures

The FeCoNi, CrFeCoNi, AlFeCoNi, and TiFeCoNi alloys (named as FCN, CFCN, AFCN, and TFCN, resp.) were prepared by arc melting using appropriate amounts of titanium, aluminum, chromium, iron, cobalt, and nickel, the purity of all of which exceeded 99.9%. Table 1 lists the compositions of the targets analyzed by inductively coupled plasma atomic emission spectrometry (ICP-AES, Jarrell-Ash, ICAP 9000). DC physical vapor sputtering (PVD) was used to deposit these metallic films. It was performed at 100 W and the flow rate of Ar was 30 standard cubic centimeters per min (sccm). The base and working pressures were 5×10^{-5} and 2×10^{-3} torr, respectively. Some of the samples were annealed using a vacuum furnace with a mechanical pump, and the working pressure was 1×10^{-2} torr. The microstructural evolutions of the thin films were monitored using scanning electron microscopy (SEM) and transmission electron microscopy (TEM). SEM observations were made using

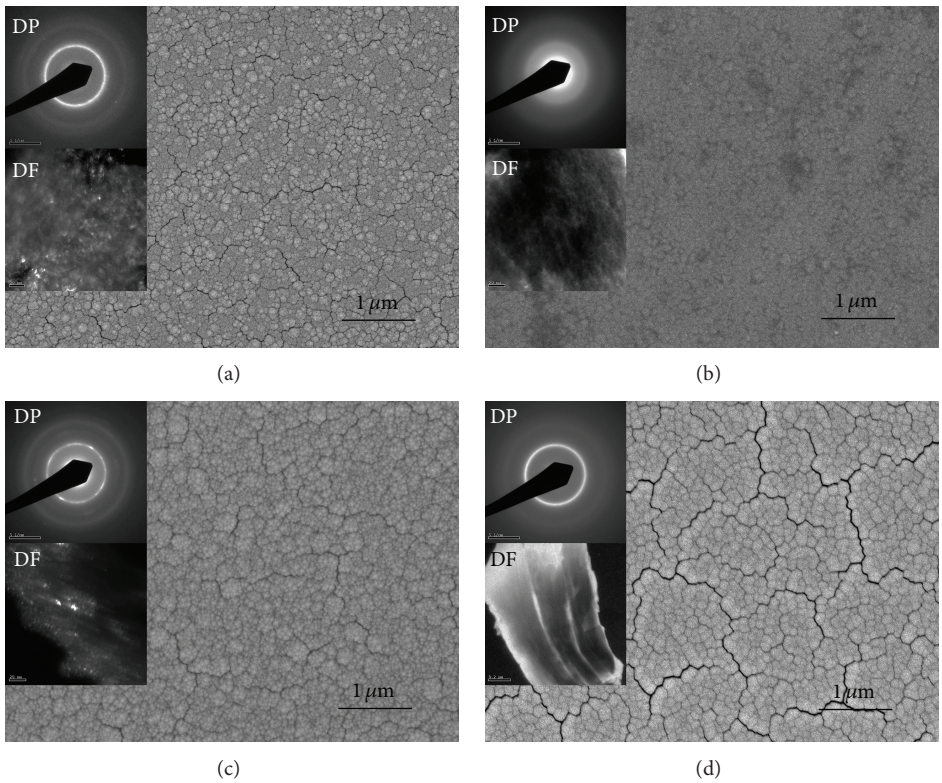

Figure 1: The plan-view micrographs of the as-deposited (a) FCN film; (b) CFCN film; (c) AFCN film; and (d) TFCN film, respectively. The insets are the corresponding SAD (marked by DP) and DF image (marked by DF) of each as-deposited thin film.

Table 1: The chemical compositions of the (Al, Cr, Ti)FeCoNi targets.

Alloys	Compositions (at.%)					
	Al	Ti	Cr	Fe	Co	Ni
FeCoNi	*	*	*	33.2	33.3	33.5
AlFeCoNi	24.8	*	*	25.2	25.1	24.9
TiFeCoNi	*	25.1	*	25.2	24.7	25.0
CrFeCoNi	*	*	25.1	24.8	25.3	24.8

a JEOL JSM-6335 field emission scanning electron microscope operated at 15 kV. TEM observations were made using a JEOL JEM-2010 transmission electron microscope operated at 200 kV. The room-temperature electrical resistivity of all samples was measured with a Napson Corporation Model TR-70 four-point probe.

3. Results and Discussion

The micrographs of the as-deposited alloy thin films are shown in Figure 1. The plan-view micrographs of the as-deposited alloy films all have a similar granular morphology. However, these structures are analyzed as an amorphous one, and the narrower black lines are amorphous grain boundaries. Donovan and Heinemann first observed these amorphous grain boundaries in an evaporated amorphous Ge thin film [15], and they suggested that the formation of a void network resulted in density-deficient boundaries that are intrinsic to amorphous films. Tsukimoto et al. further described the mechanism of formation of amorphous grain boundaries in TaN thin films, following a detailed analysis [16]. In this study, the thin films also had a similar phenomenon; the typical cross section of these thin films all had the columnar structure, shown in Figure 2. The insets of each SEM micrograph, shown in Figure 1, are the corresponding selection area diffraction pattern (SAD) and TEM dark field image (DF), respectively. The SADs proved the amorphous structures, and the DF images show the nanoscale clusters in these thin films, indicating that the as-deposited thin films

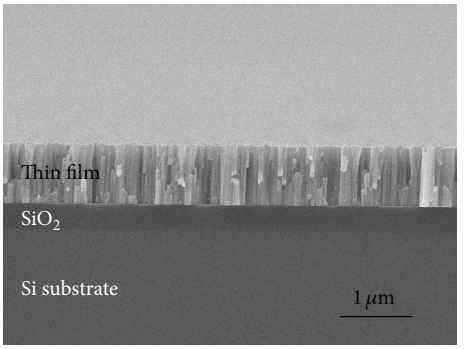

Figure 2: The cross section micrograph of the as-deposited FCN film which shows the typical columnar structure.

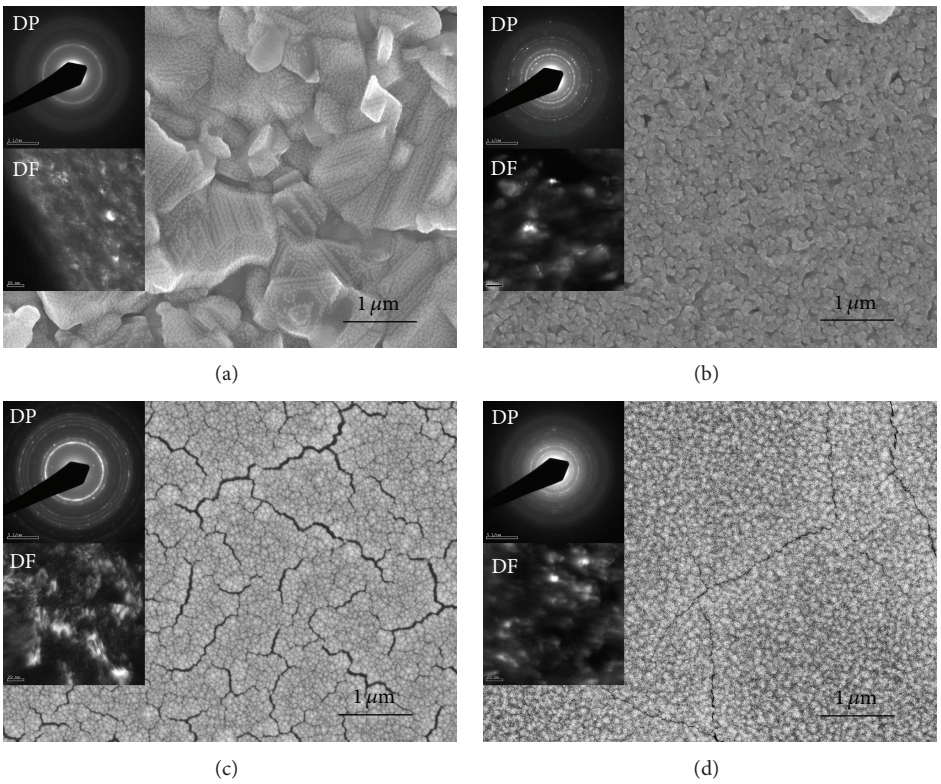

Figure 3: The plan-view micrographs of the as-annealed (a) FCN film; (b) CFCN film; (c) AFCN film; and (d) TFCN film, respectively. The insets are the corresponding SAD (marked by DP) and DF image (marked by DF) of each as-annealed thin film.

were not crystalline in structure. In addition, we observed the cracks on the surface of the as-deposited FCN, AFCN, and TFCN films, but no crack was observed in as-deposited CFCN film. The wide black lines in the SEM micrographs of the as-deposited thin films are the crack along the amorphous grain boundaries. These cracks were caused by the internal stress during the deposition process and the difference in atomic sizes. However, CoCrFeNi has single-phase solid solution, a ductile material with low hardness, and very similar atomic sizes [17, 18]. Therefore, no crack was found in this alloy thin film under as-deposited state.

These thin films became oxides after annealing at vacuum furnace at high temperature; and their morphologies also changed because of diffusion of the elements and oxidation. The plan-view of as-annealed micrographs of the $FeCoNiO_x$, $CrFeCoNiO_x$, $AlFeCoNiO_x$, and $TiFeCoNiO_x$ films (named as FCNO, CFCNO, AFCNO, and TFCNO, resp.) is shown in Figure 3. The annealing conditions are all fixed at 1000°C for 30 min. The large granular structure of the FCNO film is quite different with as-deposited morphology, shown in Figure 3(a). The CFCNO film has a particle-like structure, shown in Figure 3(b). The cracks in the AFCNO film are wider than the as-deposited condition, shown in Figure 3(c). On the contrary, the cracks in the TFCNO film are less than as-deposited state, because of the crystallization and healing of voids and cracks along amorphous grain boundaries, shown in Figure 3(d). The columnar structures of the as-deposited thin films also changed after annealing. Figure 4 shows the cross section morphology of the CFCNO film after annealing at 1000°C for 30 min, indicating this thin film became a particle-like structure. The similar result was also observed in the other three thin films.

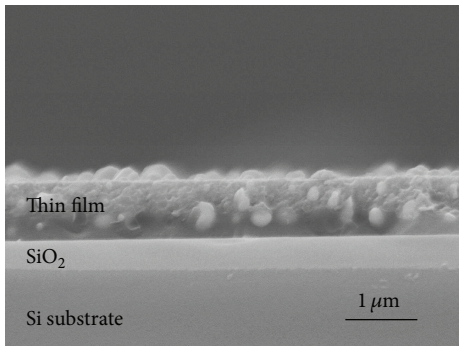

Figure 4: The cross section micrograph of the as-annealed AFCN thin film.

The resistivity of these four oxide films after vacuum annealing at different temperatures is shown in Figure 5. The annealing times were all fixed at 30 min. The resistivities of the as-deposited TFCN, FCN, AFCN, and CFCN films are 1860, 950, 175, and 98 $\mu\Omega$-cm, respectively. The as-deposited CFCN thin film had the lowest resistivity because of its uniform morphology; no crack was observed. All of these were because of their similar atomic sizes and less lattice

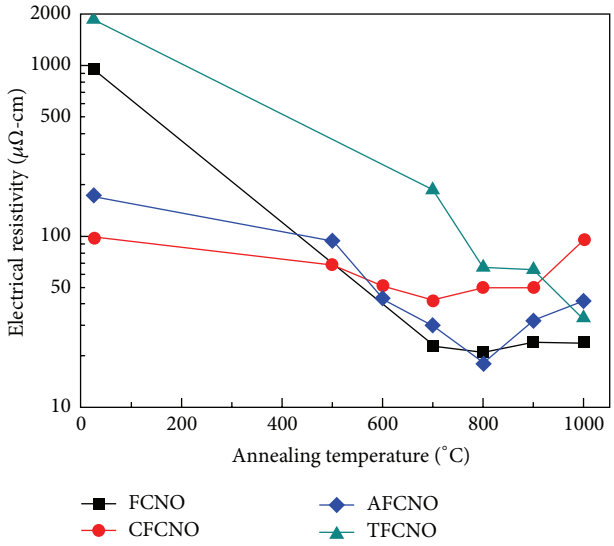

Figure 5: Plot of the resistivity of the thin films versus annealing temperature. The annealing times were all 30 min.

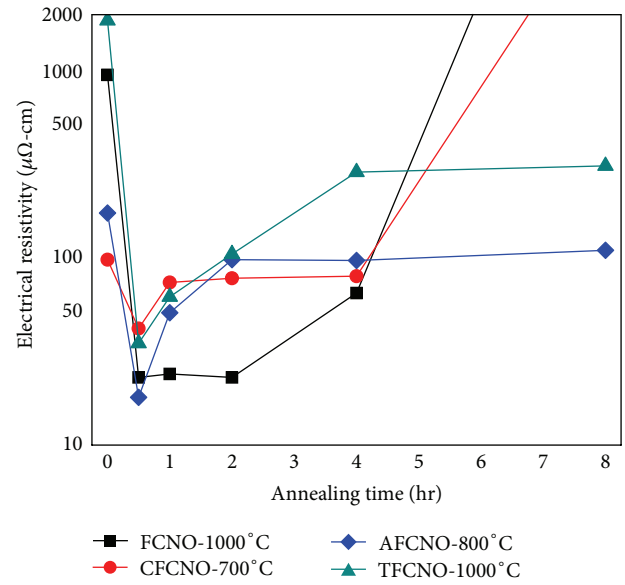

Figure 6: Plot of the resistivity of the thin films versus annealing times. The annealing temperatures for the FCNO, TFCNO, CFCNO, and AFCNO thin film were 1000°C, 1000°C, 700°C, and 800°C, respectively.

distortion [17, 18]. The other three as-deposited thin films all show that the cracks are along their amorphous grain boundaries. Therefore, the resistivity increased because of the defect. The resistivity of the thin films all decreased after annealing because of recrystallizing and eliminating of defects. We found this interesting phenomenon first in the TFCNO film; the resistivity of as-annealed TFCNO film was lower than that of the TiFeCoNi bulk alloy [1, 2]. Therefore, we further designed the other alloys to study this phenomenon. The resistivity of the TFCNO film decreased when the annealing temperature increased, and the lowest resistivity of the TFCNO was 35 $\mu\Omega$-cm after annealing at 1000°C for 30 min. The resistivity of the FCNO film also decreased after annealing, and the resistivity almost kept the same value (~23 $\mu\Omega$-cm) at the annealing temperature range of 700~1000°C for 30 min. However, the FCNO film would be easily peeled off from the substrate if the annealing temperatures were not higher than 800°C. The thin film would slightly react with the SiO_2 layer of substrate and increase their bonding under high temperature annealing. The as-deposited AFCN films had lower resistivity, and its resistivity also decreased after annealing. The lowest resistivity of the AFCNO film was 18 $\mu\Omega$-cm after annealing at 800°C for 30 min; but the resistivity of AFCNO film increased if the annealing temperature was higher than 800°C. This study also observed the aluminum-oxide rich phase on the surface after annealing at 500°C for 30 min. Therefore, each thin film had its suitable annealing condition to get the lowest resistivity. The as-deposited CFCN film had the lowest resistivity of 98 $\mu\Omega$-cm; its resistivity only slightly decreased after annealing. The lowest resistivity of the CFCNO film was 42 $\mu\Omega$-cm after annealing at 700°C for 30 min.

According to the resistivity of the thin films described above, this study chose the annealing temperatures for the FCNO, TFCNO, CFCNO, and AFCNO thin film for investigating their resistivity aging curves which were 1000°C, 1000°C, 700°C, and 800°C, respectively. The relationship between the resistivity of the thin films and the annealing times is plotted in Figure 6. All of the curves indicate that the appropriate annealing time for the thin films is 30 min at these annealing temperatures. The lowest resistivity for each thin film was got under this annealing temperature. However, the appropriate annealing times for the thin films depended on the annealing temperature. The resistivity for the thin films increases after annealing for more than 30 min. The resistivity of the FCNO thin film almost kept the same value when the annealing time was less than 2 hours; and its resistivity increased sharply after annealing at 1000°C for more than 4 hours. The resistivity of the CFCNO thin film was worse than the FCNO thin film. The oxidation resistance of the CFCNO film had not been promoted after adding chromium; and its resistivity increased significantly after annealing at 700°C for more than 4 hours. The resistivity of TFCNO films indicated that the TFCNO film had attained very low resistivity level after annealing at 1000°C for 30 min. Additionally, its resistivity increased only slightly as the annealing time increased to 60 min. The AFCNO thin film had the similar phenomenon; it had the lowest resistivity of 18 $\mu\Omega$-cm after annealing at 800°C for 30 min.

Both of the TFCNO and AFCNO films had better oxidation resistance by comparing with FCNO and CFCNO films, because the titanium or aluminum atoms would diffuse to the surface and react with oxygen, thus forming a protection layer. Figure 7 shows the EPMA mapping results. Figure 7(a) shows the cross section SEM micrograph of the TFCNO film after annealing 1000°C for 30 min; and Figures 7(b)–7(f) are the corresponding mapping of Ti, O, Fe, Co, and Ni elements. The mapping of Ti and O elements indicates a titanium-oxide rich layer on the surface of the TFCNO

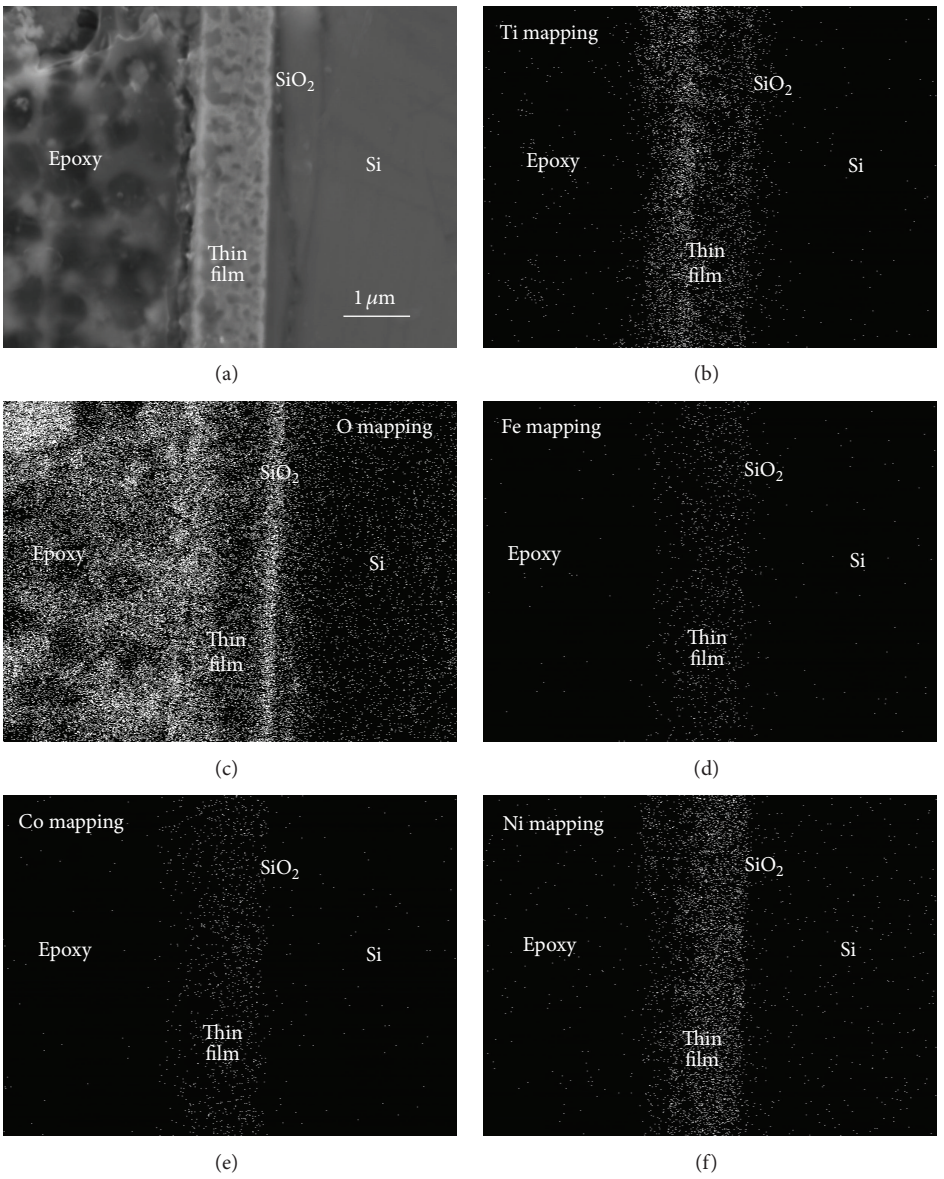

Figure 7: EPMA analyzed result. (a) The cross section SEM micrograph of the TFCNO thin film after annealing at 1000°C for 30 min and the corresponding element mapping of (b) Ti; (c) O; (d) Fe; (e) Co; and (f) Ni.

film. This phenomenon was described in our previous study [1]. During the first period of annealing, the tendency of Ti atoms to migrate significantly to the surface layer of the thin film and to form a Ti-rich oxide during annealing is clarified by comparing the Ti, Fe, Co, and Ni contents only based on metal elements. Therefore, the surface layer of TFCNO films was mostly Ti-rich oxides after annealing in a vacuum furnace for 30 min. The other three elements diffused to the surface layer and reacted with oxygen after annealing for over 30 min, and the resistivity thereby increased. The resistivity of the TFCNO film kept around 300 $\mu\Omega$-cm when annealing time increased to 8 hours. This was also contributed to the addition of titanium. Titanium element thus increased the oxidation resistance of the TFCNO film. Aluminum has the similar activity with titanium [14]. Therefore, the AFCNO film behaved similarly to the TFCNO film. The AFCNO film possessed the lowest resistivity of 18 $\mu\Omega$-cm among these films after annealing at 800°C for 30 min; and its resistivity kept around 110 $\mu\Omega$-cm when annealing time increased to 8 hours.

4. Conclusions

We used the equimolar concept to produce high-entropy $FeCoNiO_x$, $CrFeCoNiO_x$, $AlFeCoNiO_x$, and $TiFeCoNiO_x$ oxide films and studied their resistivity after annealing at different temperatures for different periods. After optimum annealing treatment, the lowest resistivity of the $FeCoNiO_x$, $CrFeCoNiO_x$, $AlFeCoNiO_x$, and $TiFeCoNiO_x$ film was 22, 42, 18, and 35 $\mu\Omega$-cm, respectively. The room-temperature

resistivity is close to that of most of the metallic alloys. The results indicated the addition of chromium had no benefit in these alloy systems. Addition of titanium or aluminum could increase their oxidation resistance, and their resistivity kept at lower values after annealing at high temperatures for long periods.

Conflict of Interests

The authors declare that there is no conflict of interests regarding the publication of this paper.

Acknowledgment

The authors would like to thank the National Science Council, Taiwan, for financially supporting part of this research under Contract no. NSC100-2221-E-034-009.

References

[1] Y. C. Yang, C. H. Tsau, and J. W. Yeh, "TiFeCoNi oxide thin film—a new composition with extremely low electrical resistivity at room temperature," *Scripta Materialia*, vol. 64, no. 2, pp. 173–176, 2011.

[2] C. H. Tsau, Y. C. Yang, C. C. Lee, L. Y. Wu, and H. J. Huang, "The low electrical resistivity of the high-entropy alloy oxide thin films," *Procedia Engineering*, vol. 36, pp. 246–252, 2012.

[3] J. Wulff, *Structure and Properties of Materials*, vol. 4, John Wiley & Sons, New York, NY, USA, 1971.

[4] W. D. Callister Jr., *Fundamentals of Materials Science and Engineering*, John Wiley & Sons, New York, NY, USA, 2nd edition, 2005.

[5] W. F. Smith, *Foundations of Materials Science and Engineering*, MaGraw-Hill, New York, NY, USA, 3rd edition, 2004.

[6] P.-K. Huang, J.-W. Yeh, T.-T. Shun, and S.-K. Chen, "Multi-principal-element alloys with improved oxidation and wear resistance for thermal spray coating," *Advanced Engineering Materials*, vol. 6, no. 12, pp. 74–78, 2004.

[7] J.-W. Yeh, S.-K. Chen, S.-J. Lin et al., "Nanostructured high-entropy alloys with multiple principal elements: novel alloy design concepts and outcomes," *Advanced Engineering Materials*, vol. 6, no. 5, pp. 299–303, 2004.

[8] J. W. Yeh, S. K. Chen, J. Y. Gan et al., "Formation of simple crystal structures in Cu-Co-Ni-Cr-Al-Fe-Ti-V alloys with multiprincipal metallic elements," *Metallurgical and Materials Transactions A*, vol. 35, pp. 2533–2536, 2004.

[9] B. Cantor, I. T. H. Chang, P. Knight, and A. J. B. Vincent, "Microstructural development in equiatomic multicomponent alloys," *Materials Science and Engineering A*, vol. 375–377, no. 1-2, pp. 213–218, 2004.

[10] C.-J. Tong, S.-K. Chen, J.-W. Yeh et al., "Microstructure characterization of Al_x CoCrCuFeNi high-entropy alloy system with multiprincipal elements," *Metallurgical and Materials Transactions A*, vol. 36, no. 4, pp. 881–893, 2005.

[11] B. Gludovatz, A. Hohenwarter, D. Catoor, E. H. Chang, E. P. George, and R. O. Ritchie, "A fracture-resistant high-entropy alloy for cryogenic applications," *Science*, vol. 345, no. 6201, pp. 1153–1158, 2014.

[12] Y. Zhang, T. T. Zuo, Z. Tang et al., "Microstructures and properties of high-entropy alloys," *Progress in Materials Science*, vol. 61, pp. 1–93, 2014.

[13] C.-H. Tsau, "Phase transformation and mechanical behavior of TiFeCoNi alloy during annealing," *Materials Science and Engineering: A*, vol. 501, no. 1-2, pp. 81–86, 2009.

[14] Z. Tang, M. C. Gao, H. Diao et al., "Aluminum alloying effects on lattice types, microstructures, and mechanical behavior of high-entropy alloys systems," *JOM*, vol. 65, no. 12, pp. 1848–1858, 2013.

[15] T. S. Donovan and K. Heinemann, "High-resolution electron microscope observation of voids in amorphous Ge," *Physical Review Letters*, vol. 27, no. 26, pp. 1794–1796, 1971.

[16] S. Tsukimoto, M. Moriyama, and M. Murakami, "Microstructure of amorphous tantalum nitride thin films," *Thin Solid Films*, vol. 460, no. 1-2, pp. 222–226, 2004.

[17] S. Guo, C. Ng, Z. Wang, and C. T. Liu, "Solid solutioning in equiatomic alloys: limit set by topological instability," *Journal of Alloys and Compounds*, vol. 583, pp. 410–413, 2014.

[18] Z. Wang, S. Guo, and C. T. Liu, "Phase selection in high-entropy alloys: from nonequilibrium to equilibrium," *JOM*, vol. 66, no. 10, pp. 1966–1972, 2014.